applied sciences

MDPI

Article

Tolerance Modeling and Analysis Considering Form Defects for Spaceborne Array Antenna

Guodong Sa [1,2], Zhenyu Liu [1,*], Chan Qiu [1] and Jianrong Tan [1]

[1] State Key Laboratory of CAD&CG, Zhejiang University, Hangzhou 310000, China; sgd@zju.edu.cn (G.S.); qc@zju.edu.cn (C.Q.); egi@zju.edu.cn (J.T.)
[2] Ningbo Research Institute, Ningbo 315000, China
* Correspondence: liuzy@zju.edu.cn; Tel.: +86-138-6747-0039

Received: 28 March 2020; Accepted: 16 April 2020; Published: 20 April 2020

Featured Application: Tolerance modeling and tolerance analysis for array antenna.

Abstract: Tolerance analysis is becoming increasingly important for tolerance design and optimization. When dealing with electromechanical products such as the array antenna, the form errors of the assembly must be considered. Traditional tolerance analysis with form errors relies on a double loop process, which is computationally expensive. A new tolerance analysis method is proposed in this paper, which can be achieved by a single loop process. First, a new tolerance modeling method considering form errors was proposed, it can represent the geometric error of a surface feature precisely. Then an effective sampling method was developed by introducing the variance separation method. An assembly simulation method was proposed to determine the final state of the whole assembly. Finally, the tolerance analysis was achieved based on the sufficient sample. The proposed analysis method was applied to an X-band spaceborne active-phased array antenna, numerical simulation results show the effectiveness of the method.

Keywords: tolerance analysis; tolerance model; form defect; array antenna; assembly simulation; tolerance sampling

1. Introduction

The manufacturing errors seriously restrict the performance of the products, and tolerance analysis plays a more and more important role for precision electromechanical product [1–3]. Based on the tolerance analysis, the effect of each tolerance variable on the product performance can be determined and then the tolerance can be optimized.

State-of-the-art tolerance analysis methods can mainly be divided into two categories: the tolerance analysis methods without form error and the tolerance analysis methods considering form errors.

(1) Tolerance analysis without form errors. Only translation and rotation errors are considered, while realistic form error (such as bending deformation) is ignored. For example, T-map method proposed by Davidson [4] maps all the possible errors of a feature to the hypothetical Euclidean volume point space, which focuses on the boundary of the Euclidean space and does not consider the specific form of a feature. Louhichi [5] proposed the discrete method to model the geometrical tolerances, all the possible translation and rotation errors are sampled by the displacements of the ideal feature. Du [6] developed the pose decoupling method for the shaft-hole fit, and studied all the possible pose of the axis within the tolerance domain.

These methods have achieved good results when dealing with traditional mechanical products, but encountered bottlenecks when dealing with the phased array antenna [7,8]. Taking the spaceborne phased array antenna as an example as shown in Figure 1a. The whole array antenna comprises of

four subarrays, the explosive view of the first subarray in the whole antenna is illustrated in Figure 1b. The performance of the antenna is determined by the realistic position (the amplitude and phase of each element is considered as ideal) of each element, details can be found in Appendix A. The position errors are mainly determined by the form errors of the reflection plate and the base plate, as a consequence, tolerance analysis without form errors cannot be applied on the antenna design. Many efficient methods such as the matrix model [9] and vector loop method [10] face the same problem.

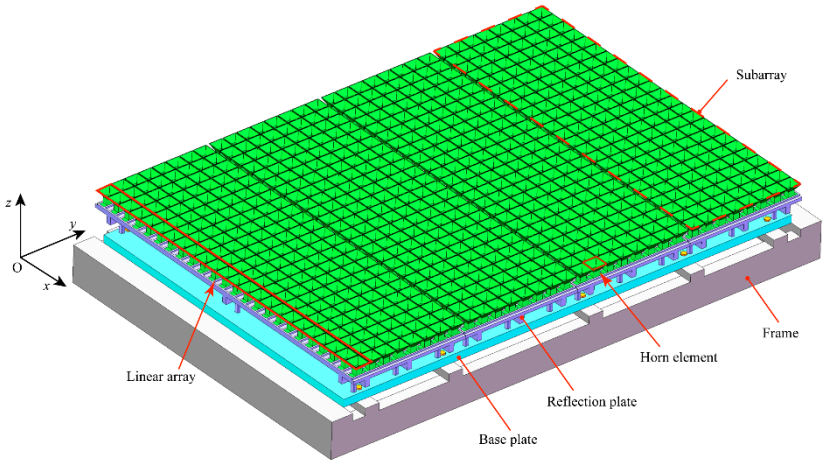

(**a**)

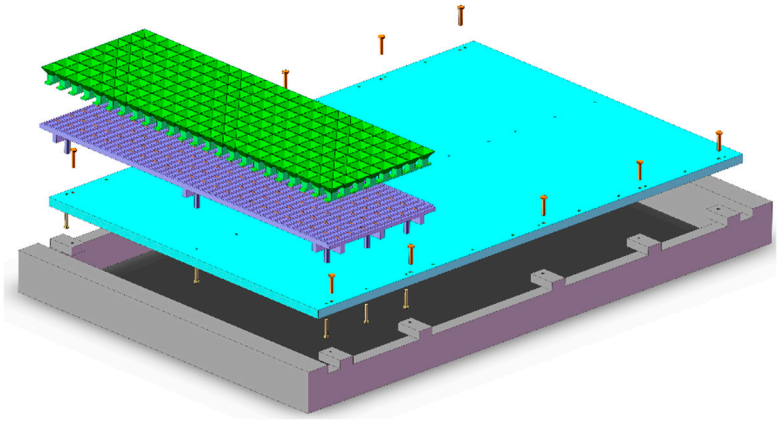

(**b**)

Figure 1. (**a**) The CAD (computer aided design) model of the spaceborne phased array antenna. (**b**) The explosive view of the first subarray in the whole antenna.

For the convenience of description, a linear array in the whole array antenna (shown in Figure 1a) was analyzed. The discrete horn element was simplified as a dot and the reflection plate was simplified as a curve, as illustrated in Figure 2a. If only the translation and rotation errors of the linear array (purple dash line in Figure 2a) are considered in tolerance analysis, then the maximum power density of the antenna will not change. However, when considering the form errors of the linear array (blue curve in Figure 2a), the maximum power density of the antenna will degenerate seriously. Figure 2b shows the relation between the maximum power density and the straightness considering form errors. The maximum power density depends not only on the size of the tolerance zone, it is also significantly

affected by the form error. Based on the engineering experience [3], the flatness of the reflection plate can be roughly estimated according to the wavelength of the antenna:

$$F \in \left[\frac{1}{30}\lambda, \frac{1}{3}\lambda\right], F: flatness,\ \lambda: wavelenght$$

For the X band spaceborne array antenna, the frequency of the electromagnetic wave is 10 GHz, and the wavelength is 30 mm. Supposing the flatness of the reflection plate is $F = \lambda/30 = 1$ mm, then the tolerance zone $[-0.5, +0.5]$ is chosen in Figure 2b.

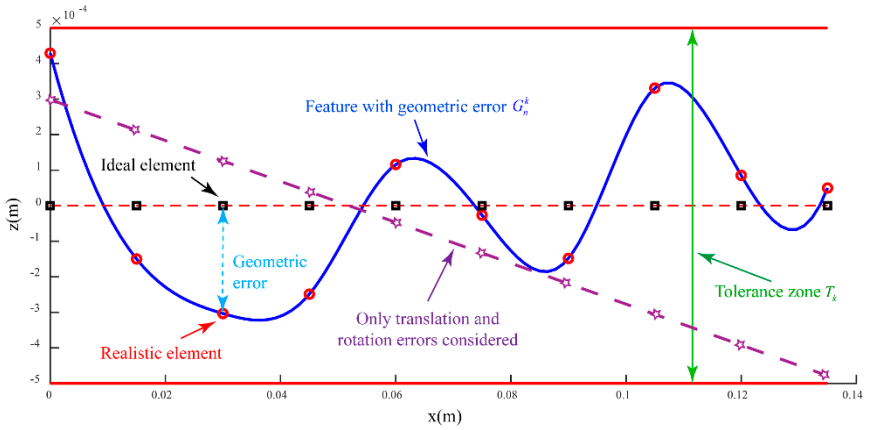

(**a**)

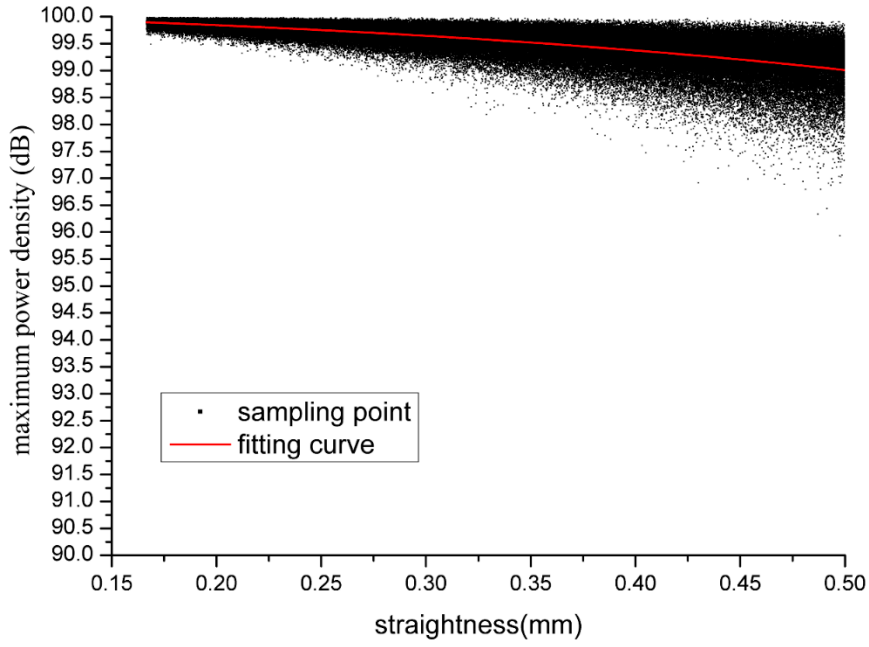

(**b**)

Figure 2. (**a**) The linear array. The black square dot represents the ideal element, and the red circular dot represents the realistic element with form error. The blue curve represents the realistic linear array while the red dotted line represents the ideal array. The purple dash line represents the linear array when only translation and rotation errors are considered. (**b**) The relation between the straightness and the maximum power density. For each sample of realistic geometric error of the linear array, the maximum power density was calculated based on Equation (A1), totally 10,000 samples were generated.

(2) Tolerance analysis considering form errors. These methods can achieve precise tolerance analysis based on the samples by applying precise tolerance model considering form errors. For example, Qiu [11] proposed the hybrid dimension-based modeling method to consider all the form errors of a face feature, such as the flatness, waviness, and roughness. Based on the hybrid dimension model, sufficient samples were generated and the tolerance was analyzed. A methodology based on Bézier curves is proposed by Zhou [12] to represent the side lines of the surface feature with flexible structural deformations, and then the assembly variation analysis was finished. A metric modal decomposition (MMD) method is developed by Homri [13] to model the form errors of various parts in a mechanism, the basic modes were defined first and the non-ideal surface was defined by the weighted sum of basic modes, then the tolerance analysis was achieved by kernel density estimation [14]. Skin model shapes were used by Anwer [15] to represent all the geometric error of the physical interface between a workpiece and its environment. He [16] proposed an assembly tolerance analysis and design method based on skin model shape. This method is highly accurate [15–17] but computationally expensive [18].

When the tolerance analysis of the linear antenna in Figure 2a is performed by the above methods, the basic process is illustrated in the left part of Figure 3. First, all the feasible values $\{T_1, \cdots T_k, \cdots T_K\}$ of the straightness are determined. Then the tolerance model was established and the samples $G^k = \left\{G_1^k, \cdots G_n^k, \cdots G_N^k\right\}$ of the geometric feature were generated for the specific value T_k (First loop, N times). The performance of the antenna was calculated based on the tolerance propagation model for all feasible values (Second loop, K times). Finally, the optimal tolerance was determined. The double loop process needs a large number of samples and is time consuming. When dealing with the complex antenna as shown in Figure 1a, the double loop process is difficult to apply.

A novel tolerance analysis method with single loop process was developed in this paper. First, the tolerance model considering form errors was developed, which can represent the geometric error of a surface feature precisely. Then the tolerance propagation was achieved efficiently based on the novel tolerance model. By introducing the variance separation method, the tolerance analysis was simplified to a single loop process. Finally, the tolerance analysis was implemented, as shown in the right part of Figure 3.

The rest of this paper is organized as follows. Section 2 discusses the novel tolerance analysis method. Section 3 discusses the numerical simulation results. Finally, Section 4 provides the concluding remarks.

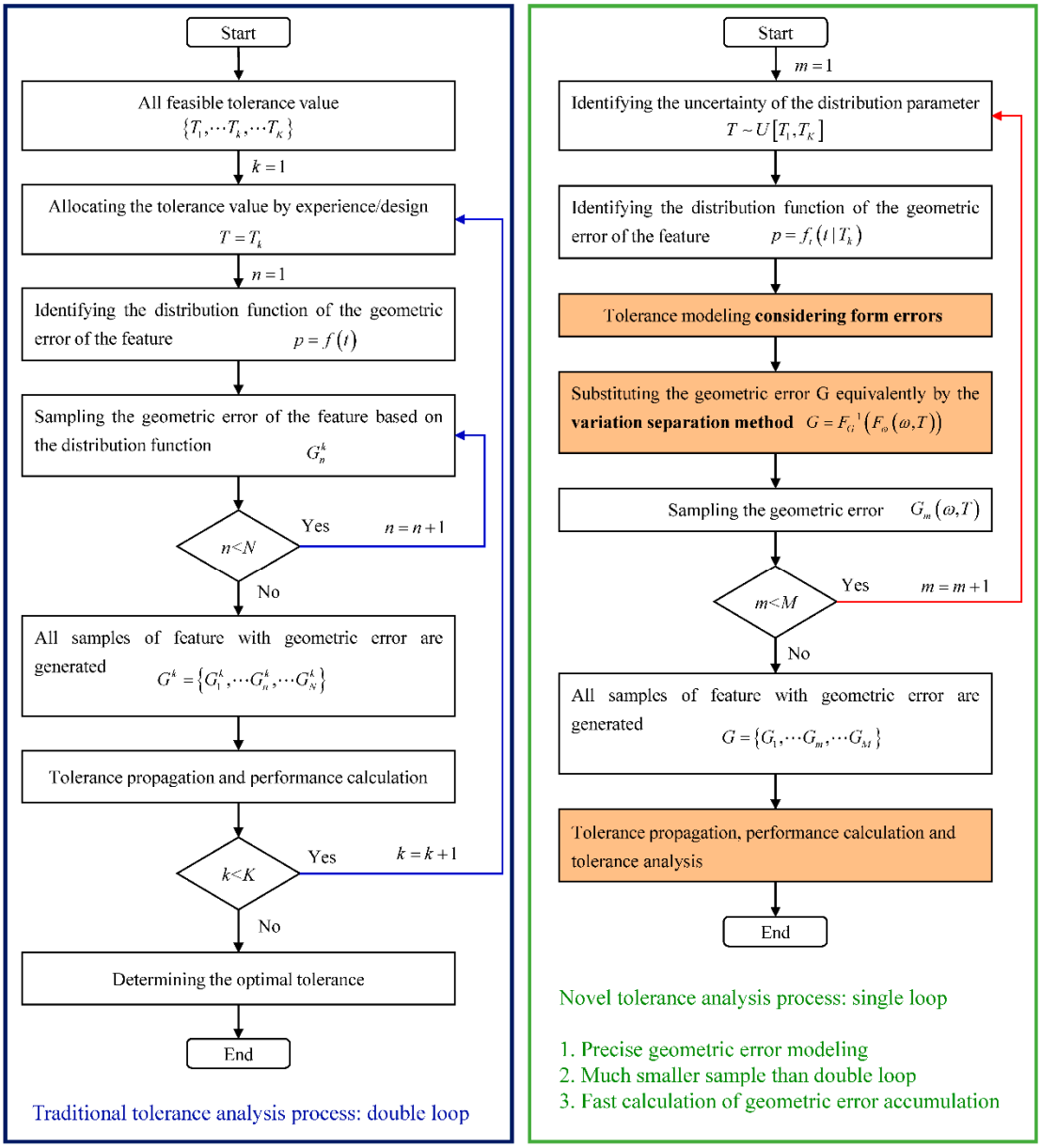

Figure 3. The process of the tolerance analysis. The left part shows the traditional tolerance analysis process, and the right part shows the novel tolerance analysis process.

2. Tolerance Analysis Considering Form Errors

The novel tolerance analysis method was developed based on Non-Uniform Rational B-Splines (NURBS) surface and the variance separation method. Compared with the traditional process, the new single loop process is much more efficient and accurate. For the convenience of description, the basic principle of the variance separation method is briefly explained first [19–21].

2.1. Variance Separation Method

Considering a model in n-dimensional space R^n.

$$y = f(x) = f(x_1, x_2, \cdots, x_n) \tag{1}$$

All the input variables $x_1, x_2, \cdots, x_n$ are independent random variables, and y is the random output. The joint probability density function (PDF) of x can be described by $f_X(x)$ with the given distribution parameters θ.

Now considering a special case, the distribution parameter θ contains uncertainty, and the uncertain of θ can be described by the PDF $f_\theta(\theta)$, where $\theta = \left(\theta_1, \theta_2, \cdots \theta_p\right)$ are p-dimensional independent variables. The uncertainty of the input variable x results from two aspects, the randomness of x itself and the uncertainty of parameter θ. Once the distribution parameter was determined, the PDF of x can be described by the conditional PDF $f_X(x|\theta)$. The family of PDFs (probability density functions) was introduced to represent the total uncertainty of variable x, as shown in Figure 4.

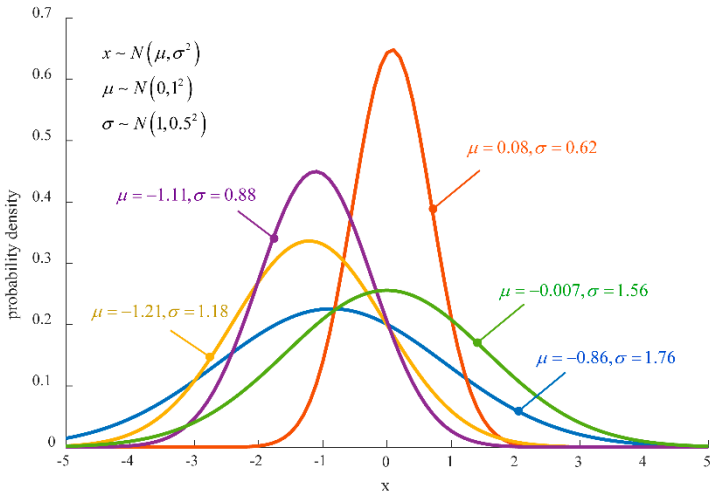

Figure 4. Family of PDFs for a single variable.

To analyze the uncertainty of y, a double-loop procedure is implemented: the sample of parameters must be generated first, then the sample of variable x can be generated. To simplify the procedure, Sankararaman [20] proposed the separation method based on the probability integral transformation (PIT) to separate the uncertainties of variables and their distribution parameters.

Denoting $F_X(x|\theta)$ as the cumulative distribution functions (CDF) of variable x, and supposing u as a standard uniformly distributed random variable, $u \sim U(0, 1)$, then based on the PIT theory, Equation (2) can be proved be true.

$$u = F_X(x|\theta) \tag{2}$$

By applying the inverse probability integral transformation, the original variable x can be represented as follow.

$$x = F_X^{-1}(u|\theta) \tag{3}$$

Then the original function Equation (1) can be transformed to Equation (4), which leads to a single-loop procedure.

$$y = f(x) = f\left(F_X^{-1}(u|\theta)\right) \tag{4}$$

Wang [21] improved the above procedure to a generalized separation method. The corresponding PIT can be given as:

$$F_\omega(\omega) = F_X(x|\theta), \quad x = F_X^{-1}(F_\omega(\omega, \theta)) \tag{5}$$

where the auxiliary variable ω is a standard random variable obeying to the same type of distribution with the original variable x. For example, if x is distributed as normal, then the auxiliary variable ω is distributed as standard normal.

Based on Equation (5), the original function Equation (1) can be described as follow.

$$y = f(x) = f\left(F_X^{-1}(F_\omega(\omega, \theta))\right) \tag{6}$$

Equations (5) and (6) are the generalized separation model from the auxiliary variable and the distribution parameter to the output, and it is more efficient than Equation (4).

2.2. Tolerance Modeling Considering Form Errors

To model the tolerance of a feature considering form errors, the geometric error of a feature must be represented precisely. A novel tolerance modeling method was proposed based on NURBS surface and the separation method. The main process of the modeling method was illustrated by taking the reflection plate in Figure 1a as example.

NURBS surface has many excellent properties, such as the affine invariance, strong convex hull property, local modification scheme, and differentiability [22]. Since all these properties perfectly satisfy the needs of flatness representation, the reflection plate with form errors is represented by a NURBS surface $S(\alpha, \beta)$ defined by Equation (7), where $N_{m,p}(\alpha)$ is the basis function in u direction and $N_{n,q}(\beta)$ is the basis function in the v direction, and $P_{m,n}(x_{mn}, y_{mn}, z_{mn})$ is the control point.

$$S(\alpha,\beta) = \frac{\sum_{m=0}^{M}\sum_{n=0}^{N} N_{m,p}(\alpha)N_{n,q}(\beta)\cdot\omega_{m,n}P_{m,n}(x_{mn}, y_{mn}, z_{mn})}{\sum_{m=0}^{M}\sum_{n=0}^{N} N_{m,p}(\alpha)N_{n,q}(\beta)\cdot\omega_{m,n}} \tag{7}$$

Defining a 5×5 grid on the NURBS surface (representing the reflection plate), each node $A_{kl}(x_{kl}, y_{kl}, z_{kl})$ was determined through measurement, as shown in Figure 5. Then the control points $P_{m,n}(x_{mn}, y_{mn}, z_{mn})$ can be calculated by global interpolation [23].

$$global\ interpolation:\ \left\{P_{1,1}, P_{1,2}, \cdots P_{m,n}\right\} = \hbar(A_{1,1}, A_{1,2}, \cdots A_{kl}) \tag{8}$$

For each sample of geometric error of the plate, the measurement points are well-determined, then the NURBS surface $S(\alpha, \beta)$ representing the reflection plate was well-determined by substituting Equation (8) into Equation (7).

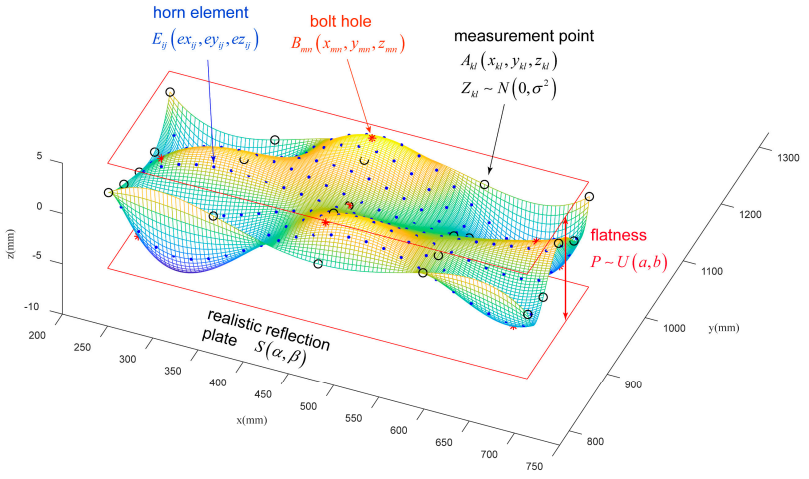

(a)

Figure 5. *Cont.*

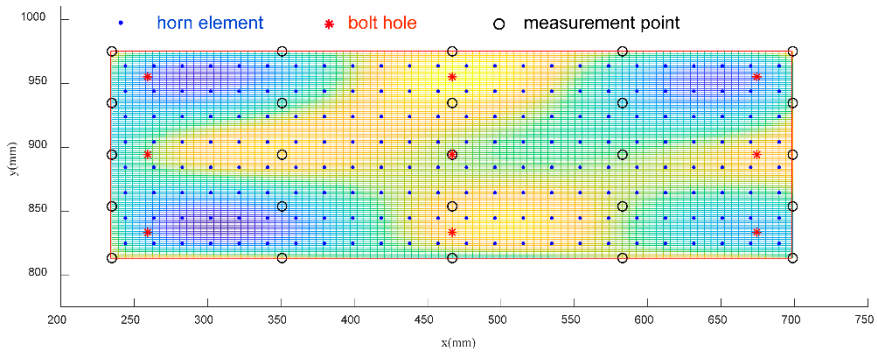

(**b**)

Figure 5. (**a**) The model of flatness. The blue points represent the discrete horn elements, the black points represent the measurement points, and the red points represent the bolt holes on the plate. The whole NURBS surface represents the realistic reflection plate, while the red rectangle borders define the tolerance zone of the flatness. (**b**) The top view of the flatness model.

Since only flatness of the reflection plate was considered, the x-directional and y-directional coordinates are assumed ideal, all the other points on the reflection plate can be then calculated by the point inversion algorithm based on the Newton iteration method [24]. For example, the horn elements E_{ij} can be determined by Equation (9). Noticing that only the z-directional coordinate ez_{ij} contains geometric error.

$$\begin{aligned} &point\ inversion: \left(\alpha_{ij}, \beta_{ij}\right) = \lambda\left(ex_{ij}, ey_{ij}\right) \\ &E_{ij}\left(ex_{ij}, ey_{ij}, ez_{ij}\right) = S\left(\alpha_{ij}, \beta_{ij}\right) \end{aligned} \tag{9}$$

The z-directional coordinate of the measurement point was assumed to be a normally distributed variable according to the manufacture.

$$z_{kl} \sim N\left(0, \sigma^2\right) \tag{10}$$

The standard deviation σ is determined by the flatness P according to the 3-sigma theory.

$$\sigma = \frac{1}{6}p \tag{11}$$

To analyze the effect of different value of P on the performance of the antenna, P was assumed as a uniformly distributed random variable.

$$P \sim U(a, b) \tag{12}$$

where a and b were constrained by the manufacture [25].

Ultimately, the uncertainty of the flatness was substituted equivalently by the uncertainty of measurement point z_{kl} and the uncertainty of the parameter σ through Equations (7)–(12).

2.3. Tolerance Sampling Method Based on Variance Separation

The main process of the sampling method was illustrated by taking the reflection plate in Figure 1a as example as well. The performance of the antenna is determined by the position of the elements, which is defined by Equation (13).

$$y = f(E) = \sum_{i=1}^{m}\sum_{j=1}^{n} a_{ij} \exp\left\{J\kappa\left(u{\cdot}ex_{ij} + v{\cdot}ey_{ij} + w{\cdot}ez_{ij}\right)\right\} \tag{13}$$

To analyze the influence of the flatness p on the performance y, the sample of flatness p must be generated first based on Equation (12), then the sample of measurement grid $A_{kl}(x_{kl}, y_{kl}, z_{kl})$ can be generated based on Equation (10), then the sample of elements $\left(ex_{ij}, ey_{ij}, ez_{ij}\right)$ can be calculated according to Equation (9), and finally, the sample of performance y can be calculated and the analysis can be achieved. This is a double-loop procedure. By introducing the variance separation method into Equation (13), the original double loop process was simplified to a single loop process.

For any value p of the flatness P, the PDF of the z-directional coordinate z_{kl} is determined by $f_{z_{kl}}(z_{kl}|p)$, the corresponding CDF is defined as $F_{z_{kl}}(z_{kl}|p)$. Supposing that:

$$u_{kl} = F_{z_{kl}}(z_{kl}|p),\ u_{kl} \sim U(0,1) \tag{14}$$

Then according to Equations (2) and (3), one can derive that

$$z_{kl} = F_{z_{kl}}^{-1}(u_{kl}, p) \tag{15}$$

According to Equations (5) and (6), the z-directional coordinate z_{kl} can be rewritten as follow.

$$z_{kl} = F_{z_{kl}}^{-1}\left(F_{\omega_{kl}}(\omega_{kl}, p)\right) \tag{16}$$

where

$$F_{\omega_{kl}}(\omega_{kl}) = F_{z_{kl}}(z_{kl}|p) \tag{17}$$

Since z_{kl} and ω_{kl} are both normally distributed variables, then based on Equations (16) and (17) one can derive that:

$$z_{kl} = \frac{1}{6}p{\cdot}\omega_{kl} \tag{18}$$

For ease of expression, the calculation of the element position based on the measurement point (Equations (7)–(9)) is abbreviated as Equation (19).

$$ez_{ij} = g(z_{11}, \cdots z_{kl}, \cdots z_{KL}) \tag{19}$$

Finally, Equation (13) can be rewritten as follow.

$$\begin{array}{l} y = f\left(ez_{11}, \cdots ez_{ij}, \cdots ez_{mn}\right) \\ ez_{ij} = g\left(F_{z_{11}}^{-1}(F_{\omega_{11}}(\omega_{11}, p)), \cdots F_{z_{kl}}^{-1}\left(F_{\omega_{kl}}(\omega_{kl}, p)\right), \cdots F_{z_{KL}}^{-1}(F_{\omega_{KL}}(\omega_{KL}, p))\right) \end{array} \tag{20}$$

Based on Equation (20), the single loop sampling method is defined clearly. First, the sufficient sample of variable ω_{kl} and P was generated, and the size of the sample is S, then the corresponding output y was calculated. Finally, the whole sample of output and input variables was achieved as shown in Equation (21).

$$\left[\begin{array}{cccc|c} \omega_{11}^1 & \cdots & \omega_{KL}^1 & p^1 & y^1 \\ \vdots & \ddots & \vdots & \vdots & \vdots \\ \omega_{11}^s & \cdots & \omega_{KL}^s & p^s & y^s \\ \vdots & \ddots & \vdots & \vdots & \vdots \\ \omega_{11}^S & \cdots & \omega_{KL}^S & p^S & y^S \end{array}\right] \tag{21}$$

The single loop process is much efficient than the original double loop process. Here is the comparison of the sample size needed in the Monte Carlo simulation by taking the reflection plate in Figure 1a as example. Supposing the simulation precision is ε, the confidence constant is c.

(1) Double loop process: First, the sample of the flatness must be generated, $\{p_1, \cdots p_k, \cdots p_K\}$, recording the sample size as K. Then for each specific flatness p_k, the realistic performance y of the antenna is randomly distributed, supposing the conditional PDF is $\psi(y|p_k)$, and the corresponding

variance is σ_k^2. According to Appendix C, the sample size needed to simulate the realistic performance y with flatness p_k is:

$$N_k \geq \frac{\sigma_k^2 c^2}{\varepsilon^2} \tag{22}$$

The total sample size D needed for the double loop process is:

$$D = \sum_{k=1}^{K} N_k \geq \sum_{k=1}^{K} \frac{\sigma_k^2 c^2}{\varepsilon^2} \tag{23}$$

(2) Single loop process: Supposing the PDF of the realistic performance y of the antenna is $\psi(y)$ in the whole design interval of flatness, $p \in [a, b]$, and the corresponding variance is σ_r^2. According to Appendix C, the sample size needed to simulate the realistic performance y is:

$$S \geq \frac{\sigma_r^2 c^2}{\varepsilon^2} \tag{24}$$

For the same simulation precision, the sample size needed in single loop process is smaller than the sample size needed in double loop process, as shown in Equation (25).

$$S = \frac{\sigma_r^2}{\sum_{k=1}^{K} \sigma_k^2} D \tag{25}$$

As the flatness increases, the variance of the antenna performance increases, that is:

$$\sigma_r^2 \leq \max\left\{\sigma_k^2\right\} \Rightarrow S < D \tag{26}$$

According to Equations (25) and (26), as the sample size K in double loop process increases, the efficiency of the single cycle process improves significantly.

2.4. Assembly Simulation Considering Form Errors

The spaceborne phased array antenna will serve in a gravity-free environment. In order to accurately predict the thermal deformation, the antenna is assembled with low stress. Therefore, only the rigid geometric error was considered here and the flexible deformation error was ignored. A simple but accurate assembly simulation method was developed in this paper to calculate the accumulation error.

The assembly process of the frame and the base plate is similar with the assembly process of the base plate and the reflection plate. They are all bolted and there is no interference between two parts. Taking the assembly of the frame and the base plate as an example, the two parts are connected by 5 pairs of bolts. When there is geometric error, the rigid assembly of the frame and the base plate is completed once 3 pairs of the 10 bolt holes contact each other.

The process of the assembly simulation method is listed as follow.

Step 1: Identifying the initial state of the frame and the base plate, the coordinates of the bolts can be calculated by Equations (7)–(9). The five pairs of bolts are illustrated in Figure 6a, the base plate (part B) is located directly above the frame (part A).

Step 2: Fixing the frame (part A), then move the base plate (part B) vertically downwards until the two parts contact each other. Recording the first contact point as C_1, that is the first bolts in contact. Recording the translation matrix as T_1.

$$T_1 = [0, 0, \min(Bz - Fz)]^T \tag{27}$$

where Bz represents the z coordinate of the bolt holes on the base plate, and Fz represents the z coordinate of the bolt holes on the Frame.

Step 3: Part B will drop down because of the gravity. Translating the origin of the coordinate system to the point C_1 by a matrix $T_2 = C_1$ first, then denoting the center of gravity of the part B as O_1, and the center of gravity of the part A as O_2. Finally, the rotation axis is defined as line L_1

$$L_1 = \frac{\overrightarrow{O_1C_1} \times \overrightarrow{O_2C_1}}{\left|\overrightarrow{O_1C_1} \times \overrightarrow{O_2C_1}\right|} \tag{28}$$

which must past point C_1, as shown in Figure 6b.

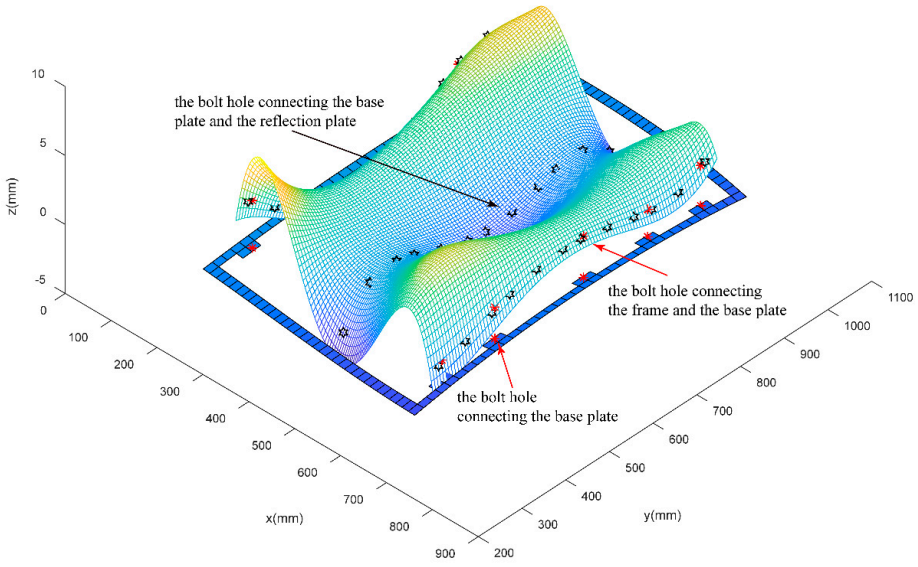

(**a**)

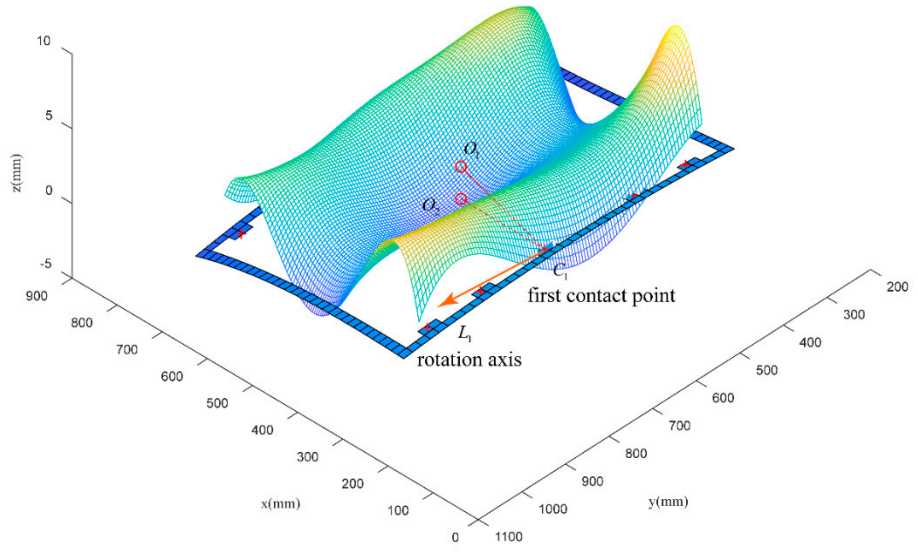

(**b**)

Figure 6. *Cont.*

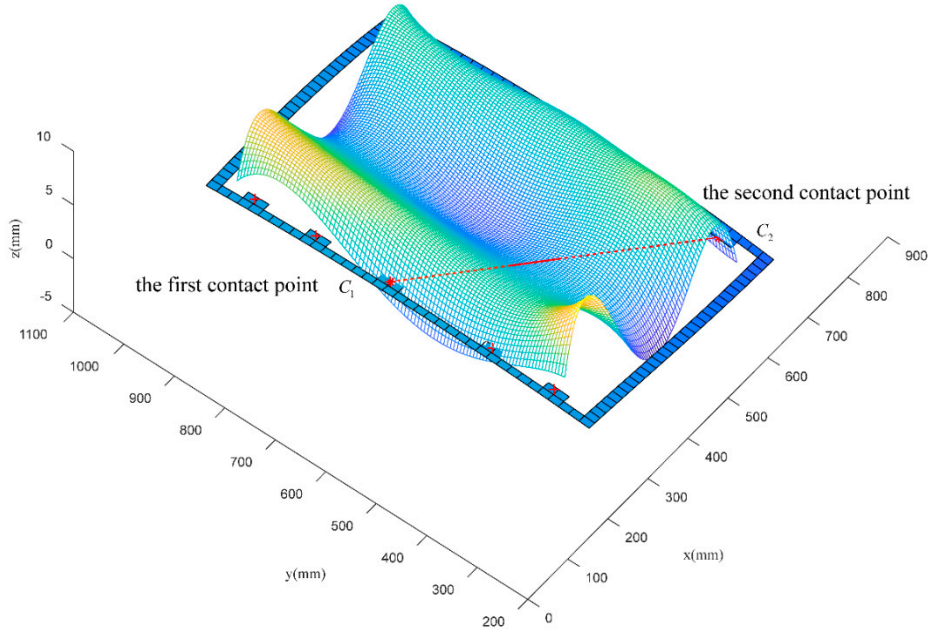

(**c**)

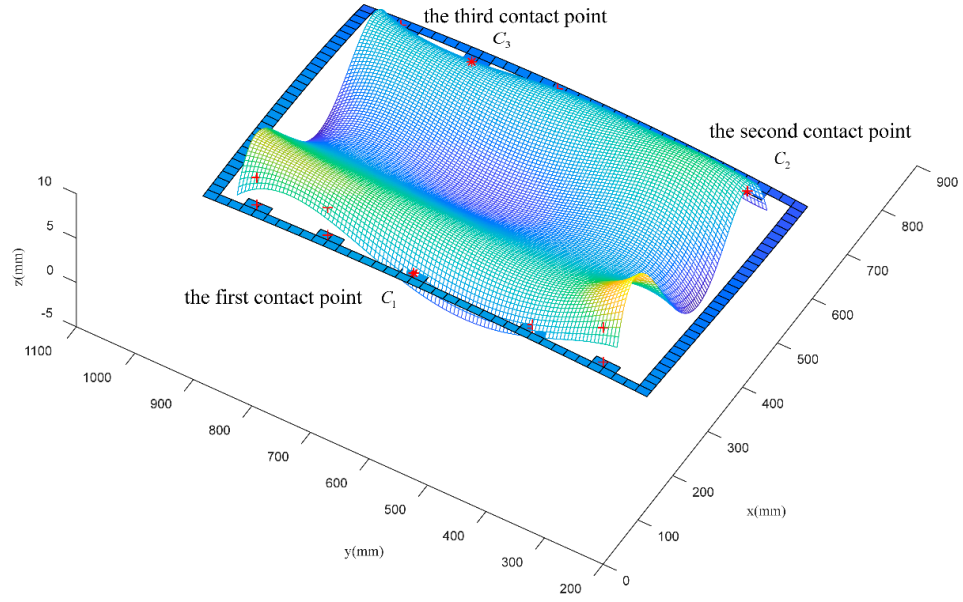

(**d**)

Figure 6. (**a**) The initial state of the frame and the base plate. (**b**) The first contact point and the rotation axis. (**c**) The second contact point and the second rotation axis. (**d**) Three contact points and the final state of the two parts.

Step 4: Rotate part B around the axis L_1 until it collides with part A. Then the second contact point C_2 is determined. Recording the first rotation matrix R_1. Details can be found in Appendix B.

Step 5: Setting line C_1C_2 as the rotation axis, as shown in Figure 6c, rotate part B until it collides with part A, then the third contact point C_3 is determined and the rigid assembly is achieved. Recording the second rotation matrix R_2.

Step 6: Substitute the rotation matrix R_1, R_2 and the translation matrix T into the NURBS model, then the final state nB of the surface is determined, as illustrated in Figure 6d.

$$nB^T = R_2R_1((B - T_1) - T_2)^T + T_2^T \tag{29}$$

The final state of all the elements can be calculated based on Equation (9), and the corresponding performance of the antenna can be calculated by Equation (13).

2.5. Tolerance Analysis Based on Samples

Based on the sample generation method in Sections 2.2–2.4, the tolerance analysis can be achieved efficiently. All the samples and corresponding performance can be illustrated by the parallel coordinates plot [15] as shown in Figure 7. All the tolerances and corresponding performance are normalized according to Equation (30) and every observation is highlighted as a connecting line; the failed observation (cannot meet the design specifications) are marked as red and the others are marked as blue.

$$T_{norm} = \frac{T - T_{min}}{T_{max} - T_{min}} \tag{30}$$

where the original tolerance design interval is defined as $[T_{min}, T_{max}]$, T represents a set of the sample, and T_{norm} represents the normalized tolerance variable.

Designers can intuitively analyze the impact of different tolerance value combinations on product performance.

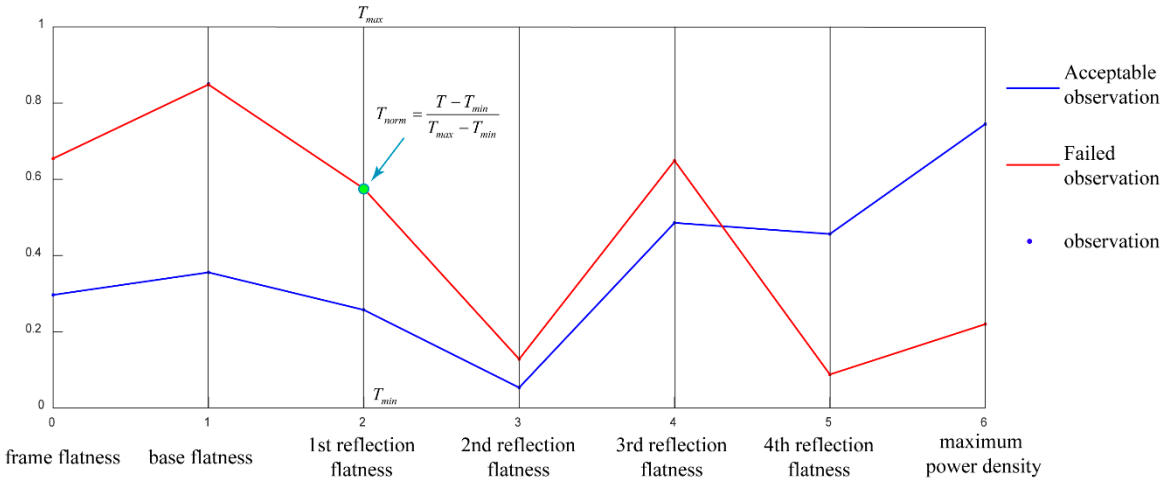

Figure 7. The parallel coordinates plot.

3. Numerical Simulation Results

The proposed tolerance analysis method was applied to an X-band spaceborne active phased array antenna, as shown in Figure 1. The whole array antenna comprises four subarrays. Each subarray consists of 8×24 elements. The base plate is affixed to the frame by 10 bolts, and the reflection plate is affixed to the base plate by 9 bolts.

A total of 100,000 sets of samples were generated for the tolerance analysis, and one of them is illustrated in Figure 8.

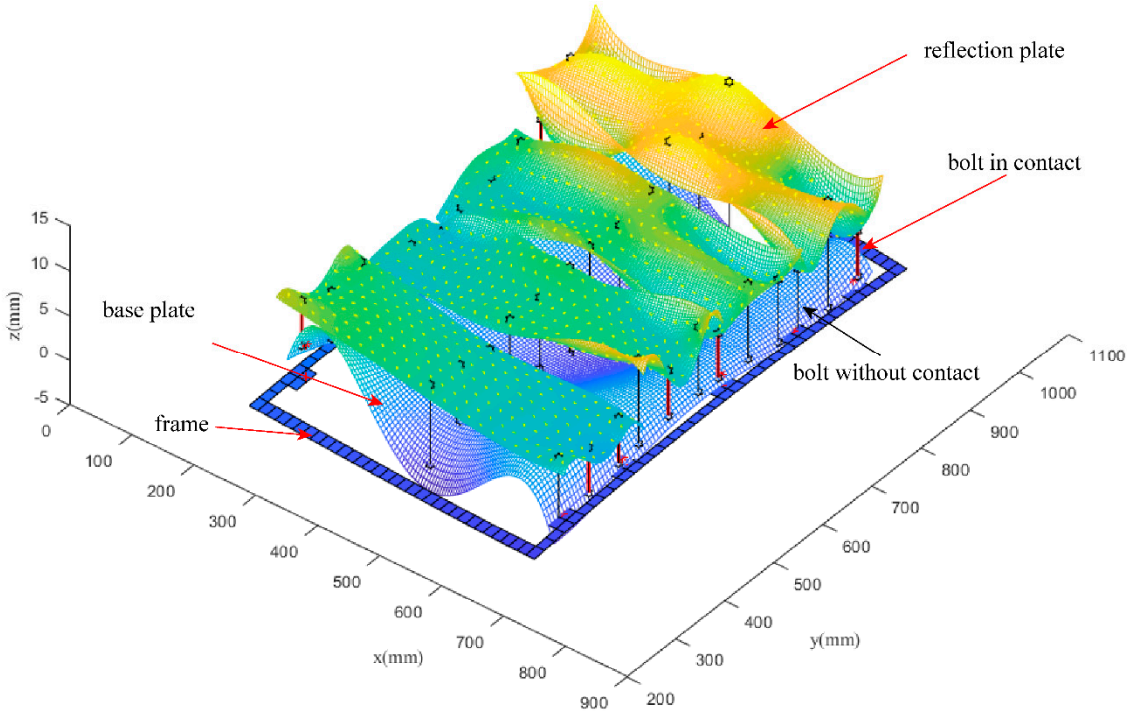

Figure 8. The final state of the whole array from a set of the samples.

The parallel coordinates plot of the samples is illustrated in Figure 9. For the sake of clarity, only 500 sets of results were drawn. The feasible design interval of each tolerance variable was divided into five intervals to analyze the failure possibility. The failure probability of the ith interval of a tolerance variable is defined as follow

$$prob_i = \frac{N^i_{red}}{N^i_{total}} \times 100\% \tag{31}$$

where N^i_{red} represents the number of the red lines passing through the ith interval, N^i_{total} and represents all the lines.

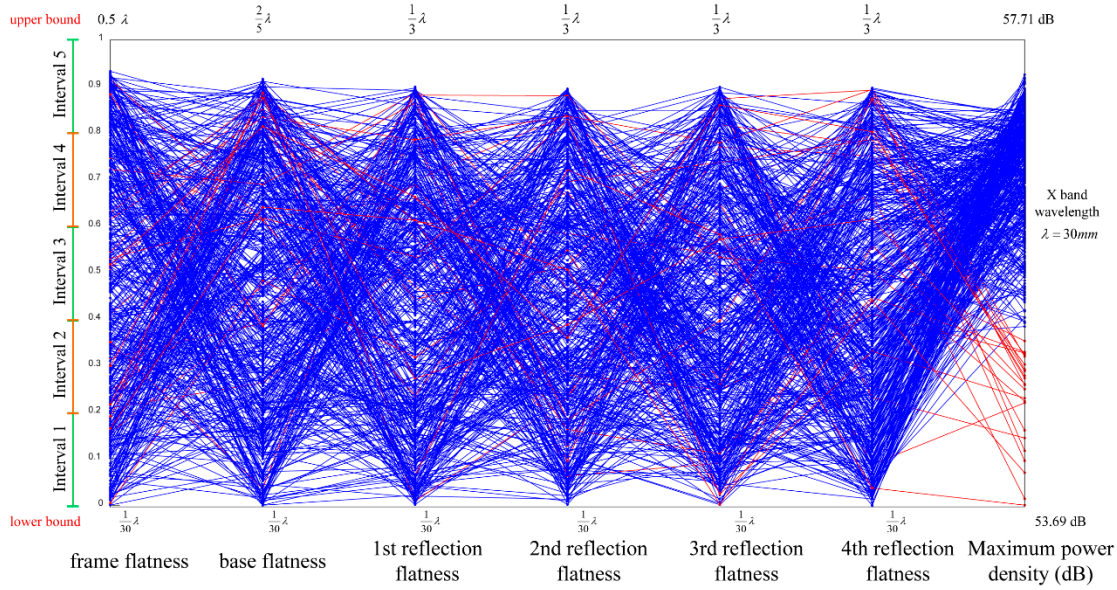

Figure 9. The parallel coordinates plot of 500 sets of samples.

The failure probability of each interval of the tolerance was illustrated in Figure 10. Results show that as the tolerance value increases, the probability of product failure increases. The maximum power density is most sensitive to the flatness of the base plate, the failure probability is 0.06% for Interval 1 and the failure probability increases to 3.25% rapidly for Interval 5. The maximum power density is not sensitive to the flatness of the frame, while the maximum power density is sensitive to the flatness of the reflection plates.

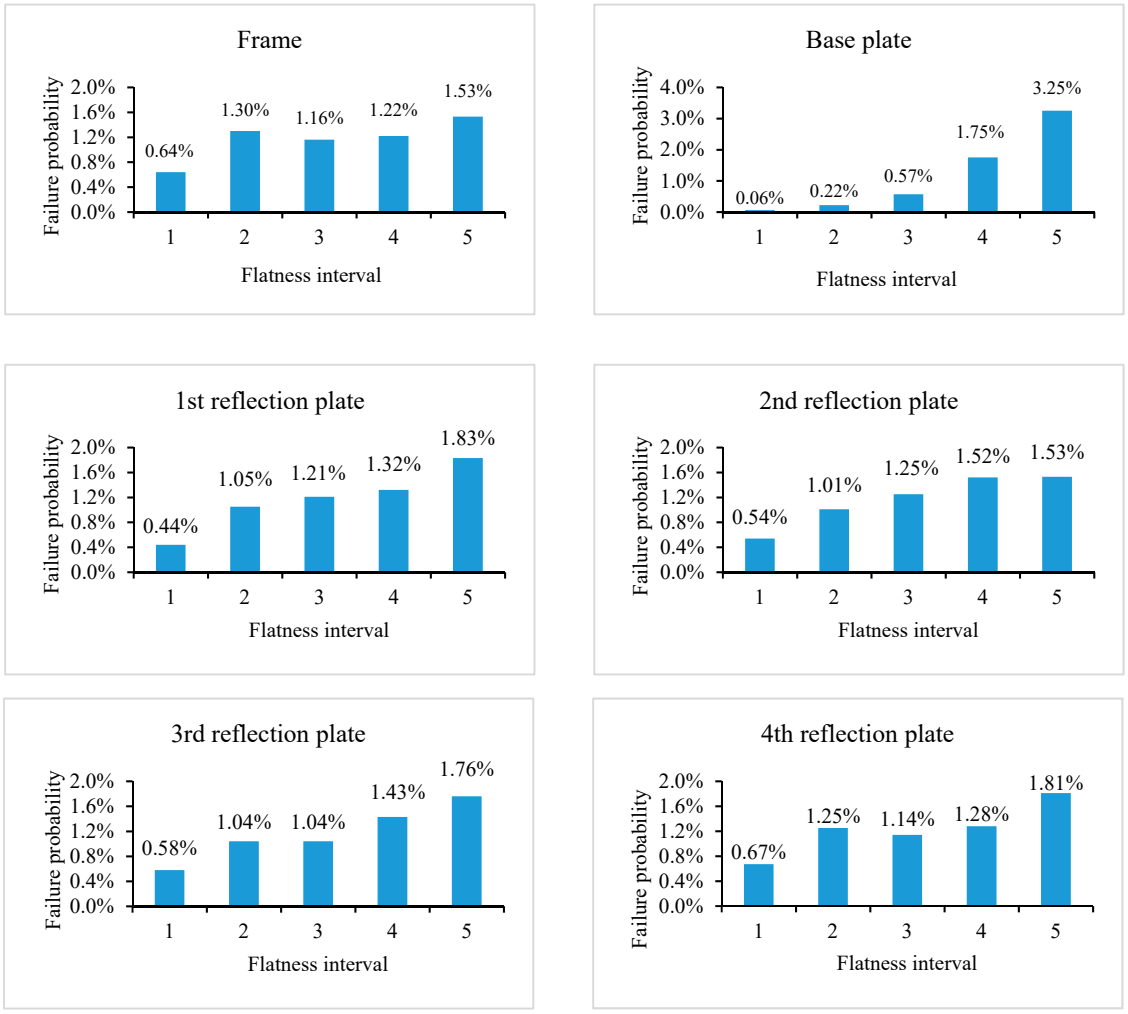

Figure 10. The failure probability of each interval of the tolerances.

The failure probability $prob_i^c$ of the combination of the six tolerance variables was calculated, which reflects the interactive effect of the six tolerance variables on the maximum power density.

$$prob_j^c = 1 - \frac{M_{blue}^j}{M_{total}^j} \times 100\% \tag{32}$$

where M_{total}^j represents the total number of the set of samples passing the specific combination of intervals. For example, one of the combinations is illustrated in Figure 11. All the sets of samples passing the interval [3,1,5,2,3,2] satisfy the requirement, which means $prob_j^c = 0\%$.

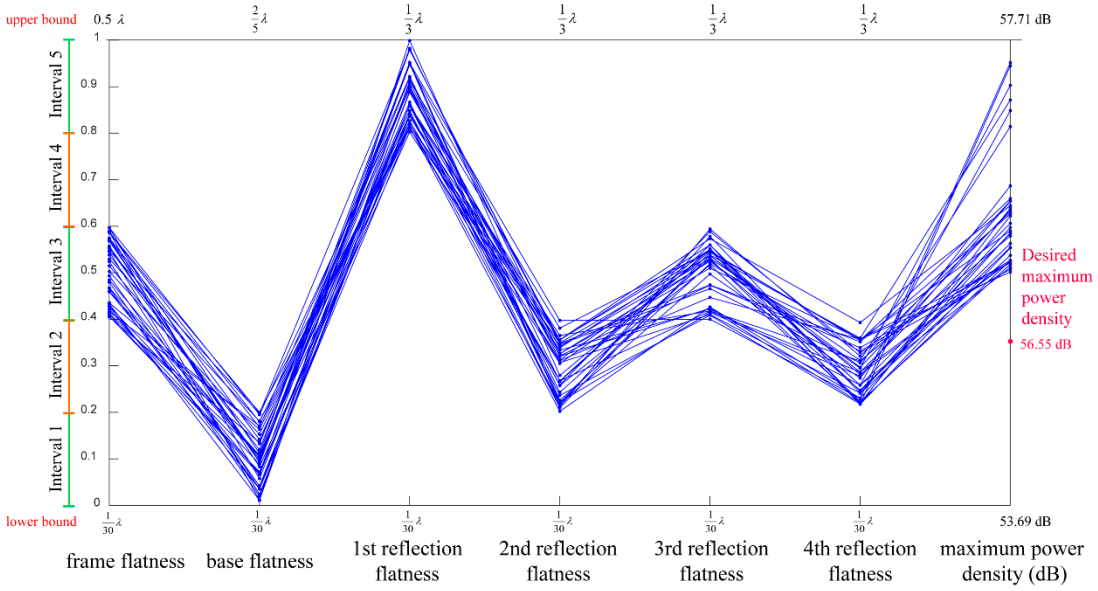

Figure 11. The parallel coordinates plot of all sets of samples passing the interval [3,1,5,2,3,2].

For cases that all the tolerances pass the strict interval, such as the interval combination [1,1,1,1,1,1], there is no need to perform the simulation, because it will lead to high costs. For cases that all the tolerances pass the loose interval, such as the interval combination [5,5,5,5,5], the failure probability must be high. Hence, only reasonable combinations are chosen, which are subjective because of the lack of accurate tolerance cost data. Finally, tolerance analysis results of three kinds of combinations are listed in Table 1 for the array antenna. The failure probability of these three kinds of combinations are very small, and the tolerances are not strict.

Table 1. Three kinds of combinations for the array antenna.

	Scheme 1		**Scheme 2**		**Scheme 3**	
Frame	Interval number	flatness interval	Interval number	flatness interval	Interval number	flatness interval
	3	$[0.22, 0.31]\lambda$	5	$[0.41, 0.5]\lambda$	4	$[0.31, 0.41]\lambda$
Base plate	Interval number	flatness interval	Interval number	flatness interval	Interval number	flatness interval
	1	$[0.03, 0.11]\lambda$	2	$[0.11, 0.18]\lambda$	2	$[0.11, 0.18]\lambda$
1st reflection plate	Interval number	flatness interval	Interval number	flatness interval	Interval number	flatness interval
	5	$[0.27, 0.33]\lambda$	3	$[0.15, 0.21]\lambda$	3	$[0.15, 0.21]\lambda$
2nd reflection	Interval number	flatness interval	Interval number	flatness interval	Interval number	flatness interval
	2	$[0.09, 0.15]\lambda$	4	$[0.21, 0.27]\lambda$	4	$[0.21, 0.27]\lambda$
3rd reflection	Interval number	flatness interval	Interval number	flatness interval	Interval number	flatness interval
	3	$[0.15, 0.21]\lambda$	2	$[0.09, 0.15]\lambda$	5	$[0.27, 0.33]\lambda$
4th reflection	Interval number	flatness interval	Interval number	flatness interval	Interval number	flatness interval
	2	$[0.09, 0.15]\lambda$	2	$[0.09, 0.15]\lambda$	4	$[0.21, 0.27]\lambda$
failure probability	0%		0%		2.12%	

Tolerance analysis can only help designers to judge whether a specific tolerance design scheme is feasible, it cannot determine the optimal scheme. Further works are needed to achieve the optimal tolerances of the spaceborne array antenna.

4. Conclusions

This study proposes an effective and accurate tolerance analysis method for complex electromechanical products. The main findings of this study are summarized as follows.

1. An accurate tolerance modelling method of surface feature was proposed, the NURBS-surface-based tolerance model can represent the form errors precisely, which will affect the performance of the antenna seriously.
2. The sampling method based on the novel tolerance model was developed by introducing the variance separation method, the traditional double-loop analysis process was then simplified to a single-loop process. This method greatly reduces the computational cost.
3. A new assembly simulation method was proposed because of the characteristics of low stress assembly. The geometric error of the whole antenna can be determined effectively. Together with the sampling method, the whole sample of product geometric error and performance can be generated precisely.
4. The tolerance analysis method was validated by a X band spaceborne array antenna. Simulation results show the effectiveness of the method.

Author Contributions: Conceptualization, Z.L. and G.S.; methodology, G.S., Z.L.; software, G.S.; validation, G.S., C.Q., and Z.L.; formal analysis, G.S.; investigation, J.T.; resources, J.T.; data curation, C.Q.; writing—original draft preparation, G.S.; writing—review and editing, G.S.; visualization, C.Q.; supervision, Z.L.; project administration, J.T.; funding acquisition, J.T. All authors have read and agreed to the published version of the manuscript.

Funding: This research was funded by National Natural Science Foundation of China, grant number 51490663, 51935009 and 51875517; Zhejiang Provincial Natural Science Foundation of China (grant No. LY20E050015).

Conflicts of Interest: The authors declare no conflict of interest.

Appendix A

The performance of a phased array antenna is described by the far field pattern [26], which is defined by Equation (A1).

$$F(\theta,\varphi)=\sum_{i=1}^{Nx}\sum_{j=1}^{Ny}a_{ij}\exp\left\{J\cdot\frac{2\pi}{\lambda}\cdot\left[(u-u_0)\cdot ex_{ij}+(v-v_0)\cdot ey_{ij}+\cos\theta\cdot ez_{ij}\right]\right\} \tag{A1}$$

where function F is the far-field pattern; coefficient a_{ij}, the element weight (amplitude and phase); $J=\sqrt{-1}$, the imaginary unit; and λ, the wavelength of the electromagnetic wave.

The position of the element with geometric error is described by coordinates ex_{ij}, ey_{ij}, and ez_{ij}, and the far field point is located at (r,θ,φ), as shown in Figure A1. The scanning angle is set to $(\theta_0,\varphi_0)=(0,0)$, which leads to $u=\cos\varphi\sin\theta, v=\sin\varphi\sin\theta$, and $u_0=0, v_0=0$.

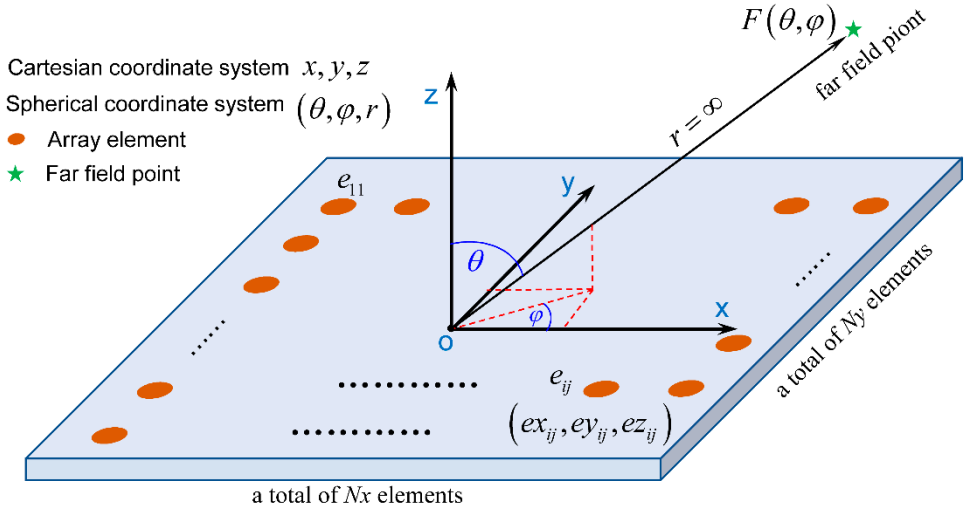

Figure A1. The pattern of the array antenna.

The maximum power density P_{max} is one of the most important performance parameters, and it is determined by the z-directional position of the elements [27]. Here we ignored the beam direction angle error since it is very small.

$$P_{max} = P(0,0) = F(0,0) \cdot F^*(0,0) \tag{A2}$$

$$F(0,0) = \sum_{i=1}^{Nx} \sum_{j=1}^{Ny} a_{ij} \exp\left\{ J \frac{2\pi}{\lambda} \cdot ez_{ij} \right\} \tag{A3}$$

Appendix B

Given a unit vector $\mathbf{u} = (u_x, u_y, u_z)$, where $u_x^2 + u_y^2 + u_z^2 = 1$, the matrix [28] of a rotation by an angle of θ about an axis in the direction of $\mathbf{u}$ is

$$R = \begin{bmatrix} \cos\theta + u_x^2(1-\cos\theta) & u_x u_y(1-\cos\theta) - u_z \sin\theta & u_x u_z(1-\cos\theta) + u_y \sin\theta \\ u_y u_x(1-\cos\theta) + u_z \sin\theta & \cos\theta + u_y^2(1-\cos\theta) & u_y u_z(1-\cos\theta) - u_x \sin\theta \\ u_z u_x(1-\cos\theta) - u_y \sin\theta & u_z u_y(1-\cos\theta) + u_x \sin\theta & \cos\theta + u_z^2(1-\cos\theta) \end{bmatrix} \tag{A4}$$

When plane B is rotated around the rotation axis $\mathbf{u}$ with the rotation angle θ, as shown in Figure A2, the original point $P_1 = (x_1, y_1, z_1)$ on plane B will be rotated to the target point $P_2 = (x_2, y_2, z_2)$ on the fixed plane A. Based on Equation (A4), we can derive that

$$P_2{}^T = R P_1{}^T \tag{A5}$$

Now considering the specific situation, point P_1 represents a bolt hole on the base plate, and point P_2 represents the corresponding bolt hole on the frame. Ignoring the x and y directional error, the necessary and sufficient condition of the contact between part A and B is

$$z_2 = \begin{bmatrix} u_z u_x(1-\cos\theta) - u_y \sin\theta & u_z u_y(1-\cos\theta) + u_x \sin\theta & \cos\theta + u_z^2(1-\cos\theta) \end{bmatrix} \cdot P_1{}^T \tag{A6}$$

where the coordinate z_2 is determined already since the frame is fixed, and the coordinate P_1 is known well in Step 1.

The rotation angle θ for assembly can be then determined by solving Equation (A6).

For each bolt hole on part B, one can calculate the corresponding rotation angle for contact, the minimum rotation angle determines the first contact point.

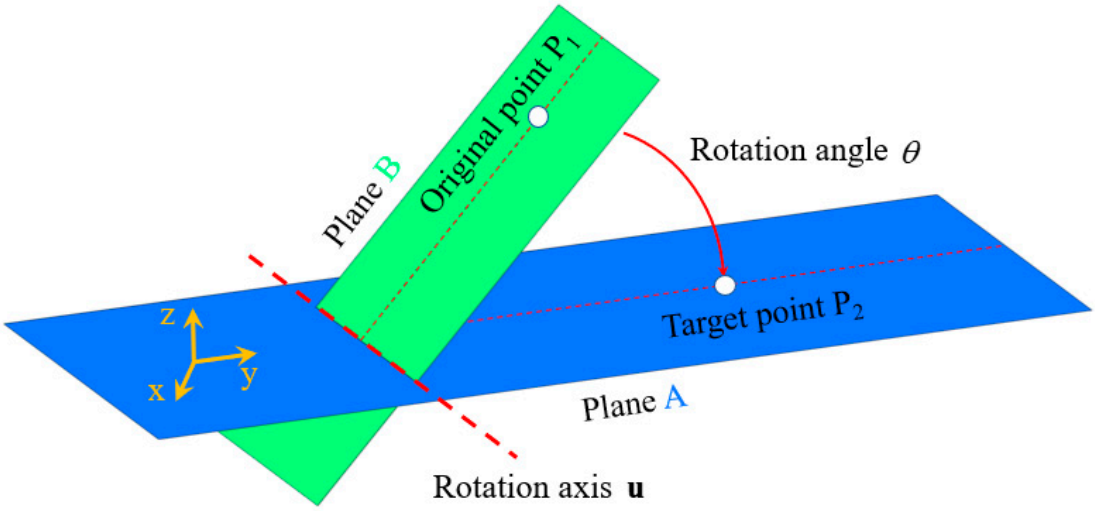

Figure A2. Rotation of a plane.

Appendix C

Given a system function,

$$y = f(x) = f(x_1, \cdots x_i, \cdots x_n) \tag{A7}$$

Supposing the joint PDF of the n-dimensional input random variables is $p_X(x)$, then the expectation of the output y is:

$$Q = E(y) = \int f(x) p_X(x) dx \tag{A8}$$

By the Monte Carlo simulation, one can estimate Equation (A8) based on the samples. Supposing totally N samples are generated:

$$\left\{x^1, \cdots x^i, \cdots x^N\right\} \tag{A9}$$

Then the expectation can be estimated by the following equation.

$$\hat{Q} = E(\hat{y}) = \frac{1}{N} \sum_{i=1}^{N} f\left(x^i\right) \tag{A10}$$

Based on the mathematical definition [29], $\hat{Q}$ is an unbiased estimator of the original Q. Given the confidence level $(1 - \alpha)$, then based on the central limit theorem:

$$\left|\hat{Q} - Q\right| \leq \frac{\sigma}{\sqrt{N}} z_{1-\alpha/2} \tag{A11}$$

where $z_{1-\alpha/2}$ is the quantile of the standard normal distribution, if $(1 - \alpha) = 0.95$, then $z_{1-\alpha/2} = 1.96$. σ is the standard variance of the function $f(x)$.

Set the quantile as a constant c, then the sample size for the Monte Carlo simulation is:

$$N \geq \left\{\frac{\sigma}{\left|\hat{Q} - Q\right|} z_{1-\alpha/2}\right\}^2 = \left\{\frac{\sigma c}{\varepsilon}\right\}^2 \tag{A12}$$

where,

$$c = z_{1-\alpha/2}, \quad \sigma = V[f(x)], \quad \varepsilon = \left|\hat{Q} - Q\right| \tag{A13}$$

Based on Equation (A12), the sample size needed in Monte Carlo simulation is determined by the confidence level, the estimation error, and the variance of the system function. The sample size is not determined by the variable dimension.

References

1. Pan, Y.; Huang, H.F.; Lei, L.; Zou, Y.; Xiao, Y.F.; Yang, T.; Xu, P. Terahertz Wideband Filter Based on Sub-Wavelength Binary Simple Periodic Structure. *Appl. Sci.* **2019**, *9*, 407. [CrossRef]
2. Choi, H.; Jo, J.-Y.; Ryu, J.-M. A Novel Focal Length Measurement Method for Center-Obstructed Omni-Directional Reflective Optical Systems. *Appl. Sci.* **2019**, *9*, 2350. [CrossRef]
3. Sa, G.; Liu, Z.; Qiu, C.; Tan, J. A Hybrid Tolerance Design Method for the Active Phased-Array Antenna. *Appl. Sci.* **2020**, *10*, 1435. [CrossRef]
4. Davidson, J.K.; Mujezinović, A.; Shah, J.J. A New Mathematical Model for Geometric Tolerances as Applied to Round Faces. *J. Mech. Des.* **2002**, *124*, 609–622. [CrossRef]
5. Louhichi, B.; Tlija, M.; Benamara, A.; Tahan, A.; Tahan, S.A. An algorithm for CAD tolerancing integration: Generation of assembly configurations according to dimensional and geometrical tolerances. *Comput. Des.* **2015**, *62*, 259–274. [CrossRef]
6. Du, Q.; Zhai, X.; Wen, Q. Study of the Ultimate Error of the Axis Tolerance Feature and Its Pose Decoupling Based on an Area Coordinate System. *Appl. Sci.* **2018**, *8*, 435. [CrossRef]
7. Hwang, S.; Sarkar, T.K. Allowable tolerances in the position of antenna elements in an array amenable to adaptive processing. *Microw. Opt. Technol. Lett.* **2004**, *43*, 215–221. [CrossRef]
8. Anselmi, N.; Manica, L.; Rocca, P.; Massa, A. Tolerance Analysis of Antenna Arrays Through Interval Arithmetic. *IEEE Trans. Antennas Propag.* **2013**, *61*, 5496–5507. [CrossRef]
9. DesRochers, A.; Riviere, A. A matrix approach to the representation of tolerance zones and clearances. *Int. J. Adv. Manuf. Technol.* **1997**, *13*, 630–636. [CrossRef]
10. Liu, Z.; Zhou, S.; Qiu, C.; Tan, J. Assembly variation analysis of complicated products based on rigid–flexible hybrid vector loop. *Proc. Inst. Mech. Eng. Part B J. Eng. Manuf.* **2018**, *233*, 2099–2114. [CrossRef]
11. Qiu, C.; Liu, Z.; Bu, W.; Tan, J. Hybrid dimension based modeling of part surface topography and identification of its characteristic parameters. *Appl. Surf. Sci.* **2012**, *258*, 7082–7093. [CrossRef]
12. Liu, Z.; Zhou, S.-E.; Cheng, J.; Qiu, C.; Tan, J.-R. Assembly variation analysis of flexible curved surfaces based on Bézier curves. *Front. Inf. Technol. Electron. Eng.* **2018**, *19*, 796–808. [CrossRef]
13. Homri, L.; Goka, E.; Levasseur, G.; Dantan, J.Y. Tolerance analysis—Form errors modeling and simulation by modal decomposition and optimization. *Comput. Aided Des.* **2017**, *91*, 46–59. [CrossRef]
14. Goka, E.; Beaurepaire, P.; Homri, L.; Dantan, J. Probabilistic-based approach using Kernel Density Estimation for gap modeling in a statistical tolerance analysis. *Mech. Mach. Theory* **2019**, *139*, 294–309. [CrossRef]
15. Schleich, B.; Anwer, N.; Mathieu, L.; Wartzack, S. Skin Model Shapes: A new paradigm shift for geometric variations modelling in mechanical engineering. *Comput. Des.* **2014**, *50*, 1–15. [CrossRef]
16. He, C.; Zhang, S.; Qiu, L.; Liu, X.; Wang, Z. Assembly Tolerance Design Based on Skin Model Shapes Considering Processing Feature Degradation. *Appl. Sci.* **2019**, *9*, 3216. [CrossRef]
17. Schleich, B.; Wartzack, S. A discrete geometry approach for tolerance analysis of mechanism. *Mech. Mach. Theory* **2014**, *77*, 148–163. [CrossRef]
18. Liu, J.; Zhang, Z.; Ding, X.; Shao, N. Integrating form errors and local surface deformations into tolerance analysis based on skin model shapes and a boundary element method. *Comput. Des.* **2018**, *104*, 45–59. [CrossRef]
19. Angus, J.E. The Probability Integral Transform and Related Results. *SIAM Rev.* **1994**, *36*, 652–654. [CrossRef]
20. Sankararaman, S.; Mahadevan, S. Separating the contributions of variability and parameter uncertainty in probability distributions. *Reliab. Eng. Syst. Saf.* **2013**, *112*, 187–199. [CrossRef]
21. Wang, P.; Lu, Z.; Xiao, S. A generalized separation for the variance contributions of input variables and their distribution parameters. *Appl. Math. Model.* **2017**, *47*, 381–399. [CrossRef]
22. Piegl, L. On NURBS: A survey. *IEEE Eng. Med. Boil. Mag.* **1991**, *11*, 55–71. [CrossRef]
23. Piegl, L.; Tiller, W.; Piegl, L. *The NURBS Book*; Springer Science and Business Media LLC: Berlin/Heidelberg, Germany, 1997.

24. Ma, Y.L.; Hewitt, W. Point inversion and projection for NURBS curve and surface: Control polygon approach. *Comput. Aided Geom. Des.* **2003**, *20*, 79–99. [CrossRef]
25. Sa, G.; Liu, Z.; Qiu, C.; Tan, J. A Novel Region-Division-Based Tolerance Design Method for a Large Number of Discrete Elements Distributed on a Large Surface. *J. Mech. Des.* **2019**, *141*, 041701. [CrossRef]
26. Mailloux, R.J. *Phased Array Antenna Handbook*; Artech House: Boston, UK, 2005; Volume 2.
27. Guo, F.; Liu, Z.; Sa, G.; Tan, J. A Position Error Representation Method for Planar Arrays. *IEEE Antennas Wirel. Propag. Lett.* **2020**, *19*, 109–113. [CrossRef]
28. Taylor, C.J.; Kriegman, D.J. *Minimization on the Lie Group SO(3) and Related Manifolds*; Technical Report No. 9405; Yale University: New Haven, CT, USA, 1994.
29. Stuart, M.; Ross, S.M. Introduction to Probability and Statistics for Engineers and Scientists. *J. R. Stat. Soc. Ser. A Stat. Soc.* **1988**, *151*, 381. [CrossRef]